Eur. Phys. J. C 48, 589–596 (2006)
DOI 10.1140/epjc/s10052-006-0018-4

THE EUROPEAN PHYSICAL JOURNAL C

Regular Article – Theoretical Physics

Electromagnetic vertex function of the pion at $T > 0$

J. van der Heide[1], E. Laermann[1,a], J.H. Koch[2,3]

[1] Fakultät für Physik, Universität Bielefeld, 33615 Bielefeld, Germany
[2] National Institute for Nuclear Physics and High-Energy Physics (NIKHEF), 1009 DB Amsterdam, The Netherlands
[3] Institute for Theoretical Physics, University of Amsterdam, Valckenierstraat 65, 1018 XE Amsterdam, The Netherlands

Received: 23 December 2005 / Revised version: 4 July 2006 /
Published online: 24 October 2006 –

Abstract. The matrix element of the electromagnetic current between pion states is calculated in quenched lattice QCD at a temperature of $T = 0.93\,T_c$. The non-perturbatively improved Sheikholeslami–Wohlert action is used together with the corresponding $\mathcal{O}(a)$ improved vector current. The electromagnetic vertex function is extracted for pion masses down to 360 MeV and momentum transfers $Q^2 \leq 2.7\ \mathrm{GeV}^2$.

1 Introduction

The theory governing the strong force, QCD, predicts distinctive changes in the behavior of hadronic matter when exposed to extreme conditions, i.e. at high temperature and/or at high baryon density. It is the aim of large experimental programs to create matter in such an environment and to study its properties. In order to interpret the experimental findings, one of the important questions to be answered is to quantify how properties of hadrons produced in heavy ion collisions are changed in a hot medium.

In this paper we investigate possible changes in the internal structure of hadrons at a temperature below the critical temperature T_c, i.e. we look for precursors of the phase transition for the pion. More specifically, we use lattice QCD to calculate spatial two- and three-point functions for a pion, to extract the pion 'form factor' at finite temperature.

Finite temperature form factors of the pion have been considered in the framework of a variety of theoretical approaches. An increase in the charge radius with increasing temperature was found in the Nambu–Jona Lasinio model [1]. Dominguez et al. [2] used a finite energy QCD sum rule to show that the charge radius of the pion increases with T and diverges at some critical temperature. An extensive study of the pion electromagnetic form factors at finite T was undertaken by Song and Koch [3] in the time-like region. Using an effective chiral Lagrangian to one loop, the form factor at $T > 0$ was found to be reduced in magnitude, in particular in the vector meson dominance region. Similar results were recently obtained by Nicola et al. [4] who work in chiral perturbation theory to one loop. They calculated the form factor in the space-like region and found that the charge radius initially stays constant, but then increases at higher temperature.

There have already been several lattice QCD investigations of some properties of a pion embedded in a heat bath. A recent review of these studies, both quenched and unquenched, can be found in [5]. Most of the work considered spatial correlators and extracted the so called 'screening masses' and spatial 'Bethe–Salpeter wave functions' of the pion. The general conclusion was that for temperatures below the phase transition temperature, T_c, there are no significant differences between the finite temperature 'screening' mass and the free pion 'pole' mass. Furthermore, the 'Bethe–Salpeter wave functions' extracted from spatial two-point correlators at $T < T_c$ were very similar to those at $T = 0$. However, as subsequent calculations [6, 7] of the pion form factor at $T = 0$ have shown, conclusions about the internal structure based on these wave functions obtained from two-point correlators are not very reliable.

We therefore study an additional observable, the three-point function of the electromagnetic current between pion states. This enables us to extract the electromagnetic vertex of the pion at $T > 0$ and to draw direct conclusions about the internal structure. We do this for a medium which has vanishing net baryon density and a temperature of $T = 0.93\,T_c$. Our study of the pion vertex function for space-like photons is the first such investigation of the spatial structure of a hadron at finite temperature with lattice QCD. For our study we use an $\mathcal{O}(a)$ improved Wilson action, together with the consistently improved vector current in order to ensure the absence of $\mathcal{O}(a)$ effects in the matrix element.

In Sect. 2, we first discuss some general features of the meson form factors at finite temperature, followed by some technical details in Sect. 3. In Sect. 4, we present the calculation of the pion two-point function and discuss our results for screening mass and dispersion relation. The pion electromagnetic vertex is then extracted from the three-point function and discussed in detail in Sect. 5. Section 6 contains our summary.

[a] e-mail: edwin@physik.uni-bielefeld.de

2 Formalism at $T > 0$

Temperature is introduced in the path integral formalism by restricting the Euclidean time direction and imposing (anti-) periodic boundary conditions. In the lattice approach, the temperature is then defined through $T = (N_\tau a)^{-1}$. To facilitate the determination of the pion form factor on the lattice, one has to calculate two observables. These are the two- and three-point Green's function of an interacting quark–antiquark pair, which carries the quantum numbers of a pion, at large separation. Since at higher temperatures the temporal direction is rather short, it becomes difficult to reliably filter out the ground state from correlators in the τ-direction and we use instead spatial correlators in the z-direction.

2.1 The two-point function

The two-point function is given by

$$G(\mathbf{x},\tau) = \langle \phi(\mathbf{x},\tau)\phi^\dagger(\mathbf{0},0)\rangle\,, \tag{1}$$

where for definiteness we assume that we are dealing with a π^+ meson,

$$\phi^\dagger(x) = \bar\psi_u(x)\gamma^5\psi_d(x)\,. \tag{2}$$

In the following, we will suppress all flavor, $SU(3)$ color and spin indices. We want to study the spatial correlator in the z-direction,

$$\tilde G(z,\tilde{\mathbf{p}}) = \int_0^{\frac{1}{T}} \mathrm{d}\tau \int \mathrm{d}x \int \mathrm{d}y \mathrm{e}^{-\mathrm{i}\tilde{\mathbf{p}}\cdot\tilde{\mathbf{x}}} G(\mathbf{x},\tau)\,, \tag{3}$$

where

$$\tilde{\mathbf{x}} = (x,y,\tau) \quad \tilde{\mathbf{p}} = (p_x,p_y,p_4) \tag{4}$$

denote the three-vector parts of the coordinates and momenta in the so called 'funny space' [8]. Due to the periodic boundary conditions for the pion, p_4 is restricted to the Matsubara frequencies,

$$p_4 = 2\pi n T \equiv \omega_n\,. \tag{5}$$

In the following we consider only the lowest contribution, $\omega_0 = 0$, since the next mode at $\omega_1 \approx 1.6\,\mathrm{GeV}$ is already quite heavy.

2.1.1 Dispersion relation and wave function renormalization

The inverse pion propagator in Euclidean momentum space can be written as

$$\Delta^{-1}(\mathbf{p},p_4;T) = \mathbf{p}^2 + p_4^2 + m^2 + \Pi(\mathbf{p}^2,p_4;T)\,, \tag{6}$$

where m is the bare pion mass, and effects due to the presence of the heat bath are incorporated into the self energy Π. In contrast to the situation at $T = 0$, the propagator can now depend separately on

$$\mathbf{p}^2 = \mathbf{p}_\perp^2 + p_z^2 \quad \text{and} \quad p_4 = n\cdot p\,. \tag{7}$$

Here, the four-velocity of the heat bath, n_μ, is given by

$$n_\mu = (0,0,0,1)\,. \tag{8}$$

In terms of the momentum space propagator in (6), the spatial correlator in the z-direction is given as

$$\tilde G(z,\tilde{\mathbf{p}}) = \int \frac{\mathrm{d}p_z}{2\pi} \mathrm{e}^{-\mathrm{i}p_z z} \Delta(\mathbf{p},p_4;T)\,. \tag{9}$$

Its behavior at large z is determined by the poles with the lowest p_z^2 value of the propagator, (6). For $p_4 = 0$, the poles occur when the spatial momentum satisfies

$$\mathbf{p}^2 = -m^2 - \Pi(-m_{\mathrm{sc},T}^2,0;T) = -m_{\mathrm{sc},T}^2\,, \tag{10}$$

where $m_{\mathrm{sc},T}$ denotes the temperature dependent screening mass. For a given value of the transverse momentum $\mathbf{p}_\perp$, the pole in p_z is therefore located at $p_{z,0}$, with

$$p_{z,0}^2 = -E_{\mathrm{sc}}^2(\mathbf{p}_\perp^2,0;T)\,, \tag{11}$$

where we have introduced the screening energy,

$$E_{\mathrm{sc}}(\mathbf{p}_\perp^2;T) = \sqrt{\mathbf{p}_\perp^2 + m_{\mathrm{sc},T}^2}\,. \tag{12}$$

The state we filter out for large separation z at a given transverse momentum $\mathbf{p}_\perp$ and $p_4 = 0$ is thus the state with the lowest *screening* energy, which satisfies the dispersion relation (10) or (12). This state is in principle different from the ground state of the pion with the lowest energy. For simplicity, however, we will refer to the state with the lowest screening energy as the 'ground state'.

In order to obtain the wave function renormalization for this state, we expand the propagator around the pole $\mathbf{p}^2 = -m_{\mathrm{sc},T}^2$. Using

$$\begin{aligned}\Pi(\mathbf{p}^2,0;T) &\cong \Pi(-m_{\mathrm{sc},T}^2,0;T)\\ &+ (\mathbf{p}^2 + m_{\mathrm{sc},T}^2)\,\frac{\partial}{\partial\mathbf{p}^2}\Pi(\mathbf{p}^2,0;T)\Big|_{\mathbf{p}^2=-m_{\mathrm{sc},T}^2} + \ldots\,,\end{aligned} \tag{13}$$

and (10), one can write the inverse propagator as

$$\begin{aligned}\Delta^{-1} &\cong (\mathbf{p}^2 + m_{\mathrm{sc},T}^2)\\ &\times \left(1 + \frac{\partial}{\partial\mathbf{p}^2}\Pi(\mathbf{p}^2,0;T)\Big|_{\mathbf{p}^2=-m_{\mathrm{sc},T}^2} + \pi_R(\mathbf{p}^2)\right)\,,\end{aligned} \tag{14}$$

where the remainder vanishes at the pole,

$$\pi_{\mathrm{R}}(-m_{\mathrm{sc},T}^2) = 0\,. \tag{15}$$

Near the pole, we therefore obtain

$$\Delta(\mathbf{p}, p_4 = 0; T) = \frac{Z}{\mathbf{p}_\perp^2 + p_z^2 + m_{\mathrm{sc},T}^2}\,, \tag{16}$$

where the renormalization constant Z is defined by

$$Z^{-1} = 1 + \frac{\partial}{\partial \mathbf{p}^2} \Pi(\mathbf{p}^2, 0; T)\bigg|_{\mathbf{p}^2 = -m_{\mathrm{sc},T}^2}\,. \tag{17}$$

2.2 The three-point function

The second observable we use is the three-point function. For the pion, using degenerate quark masses, only connected diagrams contribute. The quark–antiquark pair propagates from the source at $z_i = 0$ to the sink at z_f. The photon couples to the propagating quarks at an intermediate point z. In the continuum, this function reads in the notation introduced in (3)

$$\begin{aligned} &G_\mu(z_f, z, \tilde{\mathbf{p}}_f, \tilde{\mathbf{p}}_i) \\ &\quad = \int^{1/T} \mathrm{d}^3\tilde{\mathbf{x}}_f \int^{1/T} \mathrm{d}^3\tilde{\mathbf{x}}_i \mathrm{e}^{-\mathrm{i}\tilde{\mathbf{p}}_f\cdot(\tilde{\mathbf{x}}_f - \tilde{\mathbf{x}}) - \mathrm{i}\tilde{\mathbf{p}}_i\cdot\tilde{\mathbf{x}}} \\ &\qquad \times \langle \phi_{\mathrm{R}}(\tilde{\mathbf{x}}_f, z_f) j_\mu(\tilde{\mathbf{x}}, z) \phi^\dagger(\tilde{\mathbf{0}}, 0)\rangle\,, \end{aligned} \tag{18}$$

where j_μ is the quark vector current to which the photon couples. Details of the current will be given in Sect. 3.

2.2.1 Current structure and form factors

Given the four-vectors n, p_i and p_f, a matrix element of the electromagnetic current operator has for the pion the general Lorentz structure,

$$\begin{aligned} J_\mu &= \langle \pi(\mathbf{p}_f) | j_\mu | \pi(\mathbf{p}_i)\rangle) \\ &= e_\pi \{ (p_i + p_f)_\mu F + q_\mu G + n_\mu H \}\,, \end{aligned} \tag{19}$$

where

$$q_\mu = (p_f - p_i)_\mu \tag{20}$$

is the photon four-momentum and e_π the pion charge. The functions F, G, and H are form factors which are functions of the independent scalar variables and are subject to conditions arising from current conservation or the Ward identity. In contrast to the situation at $T = 0$ they can depend on more scalar variables, namely

$$p_i^2, p_f^2, n^2, q^2, n\cdot p_i, \quad \text{and} \quad n\cdot p_f\,. \tag{21}$$

The last two scalars amount to $p_{4,i}$ and $p_{4,f}$. When calculating the three-point function, (18), we choose to project out states with transverse momenta of the same magnitude,

$$\mathbf{p}_{\perp,f}^2 = \mathbf{p}_{\perp,i}^2 = \mathbf{p}_\perp^2\,. \tag{22}$$

By choosing large spatial separations of the vertex from both source and sink and $p_4 = 0$, we filter out the initial and final pion in the 'ground state' which satisfies the dispersion relation (12). It is therefore easily seen that the form factors with this choice of kinematics will only depend on two scalars, the screening mass $m_{\mathrm{sc},T}$ and

$$Q^2 = -q^2 = (\mathbf{p}_{\perp,f} - \mathbf{p}_{\perp,i})^2\,. \tag{23}$$

In our applications the momentum transfer to the pion, Q^2, is varied by changing the angle between $\mathbf{p}_{\perp,i}$ and $\mathbf{p}_{\perp,f}$ and by choosing different values for $\mathbf{p}_\perp^2$, (22).

Current conservation for matrix elements of the current operator between initial and final pion states yields in general

$$\begin{aligned} 0 = {} & (p_f^2 - p_i^2) F(m_{\mathrm{sc},T}^2, Q^2) + q^2 G(m_{\mathrm{sc},T}^2, Q^2) \\ & + n\cdot(p_f - p_i) H(m_{\mathrm{sc},T}^2, Q^2)\,. \end{aligned} \tag{24}$$

Since for our symmetrical kinematics $p_f^2 = p_i^2$ and $n\cdot(p_f - p_i) = 0$, we see that G must vanish. Furthermore, the term involving H will not contribute if we consider spatial components of the current. Choosing in particular the z-component, we obtain for the lattice version of the pion current

$$\begin{aligned} &\langle \pi(\mathbf{p}_{\perp,f}) | j_z | \pi(\mathbf{p}_{\perp,i})\rangle_{\mathrm{lattice}} \\ &= e_\pi F(Q^2, m_{\mathrm{sc},T}^2) \frac{p_{z,f} + p_{z,i}}{2\sqrt{p_{z,f}(\mathbf{p}_\perp^2) p_{z,i}(\mathbf{p}_\perp^2)}} \\ &= e_\pi F(Q^2, m_{\mathrm{sc},T}^2)\,. \end{aligned} \tag{25}$$

As already pointed out in [7], the cancellation of the kinematical factor in the last step due to our symmetric choice of momenta makes the extraction of the form factor F from the lattice data more reliable.

2.2.2 Effective charge

In comparison to the free pion current at $T = 0$, there are two modifications at $T > 0$. First, the overall renormalization constant Z, (17) at finite temperature, might differ from the corresponding value at $T = 0$. Secondly, the vertex operator gets modified. At the photon point, where $Q^2 = 0$ and $\mathbf{p}_{\perp,f} = \mathbf{p}_{\perp,i}$, we absorb both effects into an effective charge e_{eff},

$$\langle \pi(\mathbf{p}_\perp) | j_z | \pi(\mathbf{p}_\perp)\rangle \equiv e_{\mathrm{eff}} 2p_z\,. \tag{26}$$

The modification of the vertex can in this case be obtained from the Ward–Takahashi identity for the vertex operator j_μ,

$$(p' - p)_\mu j_\mu = e_\pi \{ \Delta^{-1}(\mathbf{p}', p_4'; T) - \Delta^{-1}(\mathbf{p}, p_4; T) \}\,. \tag{27}$$

Taking first $\tilde{\mathbf{p}}' = \tilde{\mathbf{p}}$ and then the limit $p_z' \to p_z$, one obtains at the photon point

$$j_z(Q^2 = 0) = e_\pi \frac{\partial}{\partial p_z} \Delta^{-1}(\mathbf{p}, p_4, T) = 2e_\pi p_z \left(1 + \frac{\partial}{\partial \mathbf{p}^2} \Pi(\mathbf{p}^2, 0; T)\right) .$$

When evaluating the matrix element of the vertex operator j_z between states satisfying the dispersion relation (12), we have

$$\begin{aligned} j_z(Q^2 = 0) &= 2e_\pi p_z \left(1 + \frac{\partial}{\partial \mathbf{p}^2} \Pi(\mathbf{p}^2, 0; T)\right)\Big|_{\mathbf{p}^2 = -m^2_{\mathrm{sc},T}} \\ &= 2e_\pi p_z Z^{-1} , \end{aligned} \tag{28}$$

where Z was defined in (17). The vertex correction will thus precisely cancel the wave function renormalization factor Z, resulting in

$$e_{\mathrm{eff}} = e_\pi . \tag{29}$$

Thus, if we use pion states obtained from spatial correlators, the effective charge determined from spatial components of the conserved current is the same as the free charge. This complements the remark in [3], where it was noticed that the effective charge obtained from the z-component is different from the one obtained from the t-component if the *same* wave function renormalization constant is used in both cases. This difference is due to the fact that Lorentz invariance is broken and the self energy depends separately on $\mathbf{p}$ and p_4 at $T > 0$.

3 Technical details

Most practical aspects of our lattice calculations are identical to the procedures in [7]. We therefore only give a short summary.

Our calculations were done on a $N_\sigma \times N_\tau = 32^3 \times 8$ lattice. The N_τ value corresponds to $T = 0.93\, T_{\mathrm{c}}$ at the chosen value of $\beta = 6.0$. In comparison to [7], the spatial size of the lattice has been increased from $N_\sigma = 24$ at $T = 0$ to $N_\sigma = 32$ to have the same length in the correlation direction. We generated $\mathcal{O}(200)$ configurations, twice as many as at $T = 0$, since we expect an increase in fluctuations in the vicinity of the phase transition.

To facilitate comparison with the results in [7], we used the same five κ values,

$$\kappa = 0.13230, 0.13330, 0.13380, 0.13430, 0.13480 , \tag{30}$$

which correspond to pion masses of 360–970 MeV[1] at $T = 0$. The action we use is the Sheikholeslami–Wohlert action [10] with the non-perturbatively determined [11] value $c_{\mathrm{SW}} = 1.7692$, which is exact to order $\mathcal{O}(a)$.

[1] We use $a = 0.105$ fm from [9] to set the scale.

In order to obtain matrix elements of the current that are correct to order $\mathcal{O}(a)$, we have to use the appropriate vector current for the chosen action. This improved vector current is [12–14]

$$j_\mu^I = Z_V \{ j_\mu^L + a c_V \partial_\nu T_{\mu\nu} \} , \tag{31}$$

where

$$j_\mu^L = \bar{\psi}(x) \gamma_\mu \psi(x) \tag{32}$$

is the local quark current, and

$$T_{\mu\nu} = \bar{\psi}(x) \sigma_{\mu\nu} \psi(x) . \tag{33}$$

In choosing this structure for j_μ^I, we have dropped terms that can be eliminated by the quark equation of motion, just as at $T = 0$. This improved current guarantees that on-shell matrix elements only have $\mathcal{O}(a^2)$ errors. For comparison, we also use the conserved lattice current [15], in our calculations

$$\begin{aligned} j_\mu^C = {} & \bar{\psi}(x)(1 - \gamma_\mu) U_\mu(x) \psi(x + \hat{\mu}) \\ & - \bar{\psi}(x + \hat{\mu})(1 + \gamma_\mu) U_\mu^\dagger(x) \psi(x) , \end{aligned} \tag{34}$$

which has $\mathcal{O}(a)$ discretization errors away from the forward direction. To enhance the contribution from the pion ground state at the sink point $(\tilde{\mathbf{x}}_f, z_f)$, we use an extended operator ϕ_{R} with a suitably chosen inter-quark distance R. To keep the calculation gauge invariant, the separated quarks at the sink are connected by gauge links which are 'fuzzed' to simulate the tube-like nature of the gluon cloud. In these steps we follow the scheme developed by Gupta et al.[16] and Lacock et al. [17]; the fuzzed gluon links at the pion sink are created with a link/staple mixing of 2 and a fuzzing level of 4. Fuzzing was performed in all three directions orthogonal to z. As a measure for the effectiveness of this method, we used the speed with which the effective screening energy,

$$E^{\mathrm{eff}}_{\mathrm{sc},T}(z, \tilde{\mathbf{p}}) = \ln \frac{\langle \tilde{G}_{\mathrm{R}}(z, \tilde{\mathbf{p}}) \rangle}{\langle \tilde{G}_{\mathrm{R}}(z+1, \tilde{\mathbf{p}}) \rangle} , \tag{35}$$

stabilizes for increasing z. We varied the quark separation R and found that, just as at $T = 0$, the value $R = 3$ was optimal. The same R was also used for the three-point functions.

4 Results for the two-point function

In order to extract information from the lattice data, the two-point function, (3), is parameterized, with $p_4 = 0$, as

$$\begin{aligned} \tilde{G}_{\mathrm{R}}(z, \mathbf{p}_\perp) = {} & \sum_{n=0}^{1} \sqrt{Z^n_{\mathrm{R}}(\mathbf{p}_\perp^2) Z^n_0(\mathbf{p}_\perp^2)} \\ & \times \mathrm{e}^{-E^n_{\mathrm{sc}}(\mathbf{p}_\perp^2) N_z/2} \cosh\left[E^n_{\mathrm{sc}}(\mathbf{p}_\perp)\left(\frac{N_z}{2} - z\right)\right] , \end{aligned} \tag{36}$$

where $N_z = 32$ is the extension of the lattice in the z-direction. The cosh structure is due to the periodic boundary conditions in z. The quantities $Z^n_{\rm R}$ denote the matrix elements $|\langle\Omega|\phi_{\rm R}|n, \mathbf{p}_\perp\rangle|^2$, the overlap between the trial state $\phi^\dagger_{\rm R}|\Omega\rangle$ and the pion state with screening energy $E^n_{\rm sc}(\mathbf{p}^2_\perp)$ and momentum $\mathbf{p}_\perp$. Since we use smearing techniques at the sink to suppress higher excited states, the parameterization can be restricted to two states. For a given momentum $\mathbf{p}_\perp$, the parameters we fit for each state are thus the screening energy, $E^n_{\rm sc}$, and the product of the amplitudes, $Z^n_{\rm R} Z^n_0$, in (36). For the momenta, we choose

$$\mathbf{p}^2_\perp = 0, 0.039, 0.077, 0.154, 0.193\,, \tag{37}$$

which are integer multiples of $p^2_{\rm min}$, where $p_{\rm min} = \frac{2\pi}{N_\sigma}$. These values include the momenta used for our form factor calculation. For each nonzero value of $\mathbf{p}^2_\perp$ we use several $\mathbf{p}_\perp$ with different directions in the $\{x, y\}$ plane. On the lattice there is still some rotational symmetry left, and the two-point function is independent of the direction of the transverse momentum. We therefore average over all momenta with the same length to increase the stability of the data.

There might still be correlations between different configurations. To deal with these, we obtained all our results using the jackknife method [19, 20].

4.1 Screening masses and dispersion relation

The results for the screening masses, $m_{{\rm sc},T}$, obtained for $\mathbf{p}_\perp = \mathbf{0}$, are given in Table 1. Also shown in the table are the free pion masses, m_π, obtained for the same action at $T = 0$ in [7]. As can be seen, the screening masses agree with the corresponding pole masses at zero temperature within error bars. This confirms earlier work [21, 22], where no significant differences between screening and zero temperature pole masses were found for a π meson at temperatures below $T_{\rm c}$; similar observations were also made for the ρ meson.

In order to investigate the dispersion relation for the lattice states, we plot the screening energies as function of the transverse momentum in Fig. 1. The screening energies obey the continuum dispersion relation, (12), quite well. This nicely confirms that lattice artifacts are largely suppressed since we are working with an improved action which only receives corrections in $\mathcal{O}(a^2)$. The error in $E_{\rm sc}(\mathbf{p}_\perp)$ grows with increasing momentum and decreasing pion mass. Due to large fluctuations, reliable results for the lowest pion mass could not be obtained at the two highest momenta.

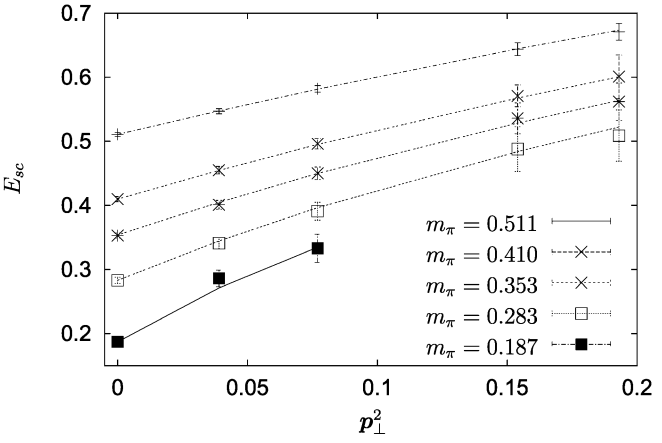

Fig. 1. $E_{\rm sc}(\mathbf{p}^2_\perp)$ for different pion masses; lines: continuum dispersion relation (12)

Table 1. Fit results at $T = 0.93T_{\rm c}$ compared to corresponding data at $T = 0$

(a) Pion masses

κ	$m_{{\rm sc,T}}$	m_π $(T = 0)$
0.13230	0.511(3)	0.516(2)
0.13330	0.410(4)	0.414(2)
0.13380	0.353(4)	0.356(2)
0.13430	0.283(5)	0.287(3)
0.13480	0.187(8)	0.194(4)

(b) VMD fit parameter m_V compared to the free ρ-mass

κ	m_V	$m_V(T = 0)$	m_ρ [18]
0.13230	0.574(11)	0.587(19)	0.623(2)
0.13330	0.520(13)	0.528(17)	0.550(2)
0.13380	0.495(15)	0.501(19)	0.515(3)
0.13430	0.466(18)	0.477(21)	0.485(3)
0.13480	0.431(25)	0.454(43)	0.448(13)

5 The three-point function and the vertex function F

For the three-point function, we consider a pseudo-scalar source at $z_i = 0$, a sink at z_f, and a coupling of the photon at $0 < z < z_f$. As was discussed in [7], for $T = 0$, the most reliable method to extract the form factor is the use of simultaneous fits of the two- and three-point functions. Consequently, this will also be the method used in this case. In analogy to the zero temperature analysis, we have varied the fit range in both correlation functions to investigate systematic uncertainties. We found no significant changes in the ground state parameters.

We carried out our simulations for the five κ values in (30), corresponding thus to the different screening masses in Table 1a. Furthermore, we chose three external momenta, $\mathbf{p}^2_\perp = 0.039$, 0.077 and 0.0193. As can be seen from our discussion in Sect. 2.2, we do not expect a dependence on $\mathbf{p}^2_\perp$ for our specifically chosen kinematical situation. The data sets for the different transverse momenta will therefore yield an indication of numerical instabilities in our results. For the lowest pion mass and highest $\mathbf{p}^2_\perp$, fluctuations overwhelmed the data and we did not extract the parameters of the three-point function.

As shown above, for our kinematics and by considering the z-component of the current, the resulting matrix element takes on a very simple structure with only one single vertex function F, which depends on Q^2 and the screening mass. In our calculations, we have considered three choices

of the current operator on the lattice: the conserved current, (34), the renormalized local current, (32), and the improved current, (31). At $Q^2 = 0$, for periodic boundary conditions, the three-point function calculated with a conserved current should satisfy the relation [23]

$$\frac{G_3(z_f, z; \tilde{\mathbf{p}}, \tilde{\mathbf{p}}) - G_3(z_f, z', \tilde{\mathbf{p}}, \tilde{\mathbf{p}})}{G(z_f, \tilde{\mathbf{p}})} = 1\,, \tag{38}$$

where $z_f < z' < N_\sigma$. In this form, the current operator is inserted twice to measure two separate contributions to the total charge reaching the sink at z_f. The first takes into account the charge from the source reaching the sink by passing through z. The 'second insertion' at z' accounts for the charge that leaves the source in the negative z-direction and arrives at the sink by passing through z', which is possible due to the periodic boundary conditions. We have confirmed that for the conserved current (38) is satisfied to high accuracy, typically to $\mathcal{O}(10^{-4})$.

For both the local and the improved current we need the overall renormalization constant Z_V,

$$Z_V = Z_V^0(1 + b_V m_q)\,. \tag{39}$$

We have determined it by demanding that (38) is satisfied. Since the additional tensor term in the improved current is a total divergence, it does not contribute to the total charge, and therefore Z_V is identical for the local and improved current. Figure 2 shows the Z_V values we obtain for several κ and $\mathbf{p}_\perp^2$ values. The higher momenta are more problematic for the extraction of the vertex functions. They have larger error bars and the extracted Z_V values tend to lie slightly higher than the lower momentum values. As the figure shows, the $T = 0.93\,T_c$ results deviate by less than 2% from $T = 0$ values extracted in [7]. They also have the same linear dependence on the quark mass. Thus, our values for Z_V^0 as well as b_V are in very good agreement with the non-perturbative determination of Bhattacharya et al. [24]. The constant c_V multiplies a term that is already linear in a. A variation with T would be of higher order, and we use the c_V value of [24] for the vector current, which contributes to the vertex only away from the forward direction.

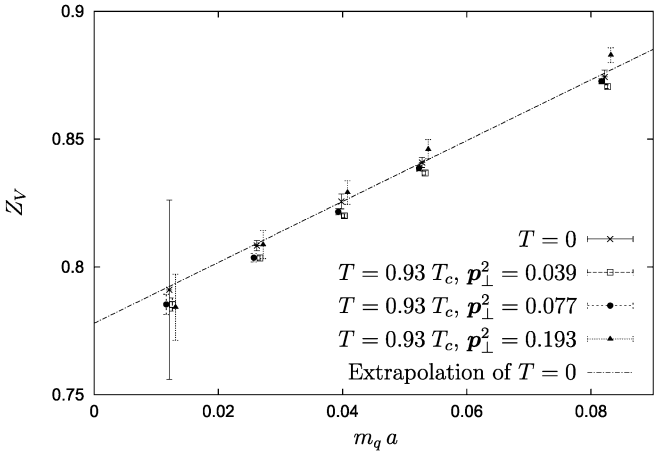

Fig. 2. Renormalization constants Z_V as function of quark mass for different T and $p_\perp$

5.1 Results for the vertex function F

We now discuss the values for the vertex function we extracted with the improved current for different photon momenta Q^2. At $T = 0$, it was found that a monopole parameterization of the pion charge form factor described the obtained results quite well for the lower Q^2 values, a feature which can be explained by the vector meson dominance (VMD) model. We investigated if the analogous parameterization,

$$F(Q^2, m_{\mathrm{sc},T}^2) = \left[1 + \frac{Q^2}{m_V^2}\right]^{-1}\,, \tag{40}$$

where m_V is a fit parameter, also yields a useful description for the vertex function we extract at $T > 0$. We therefore plot $1/F$, which should be a straight line for the parameterization to work.

As can be seen in Fig. 3 for two values of the pion screening mass, our numerical results show that for Q^2 up to 0.4 a monopole fit will work quite well. At higher Q^2, the lighter mass shows a stronger deviation from a straight

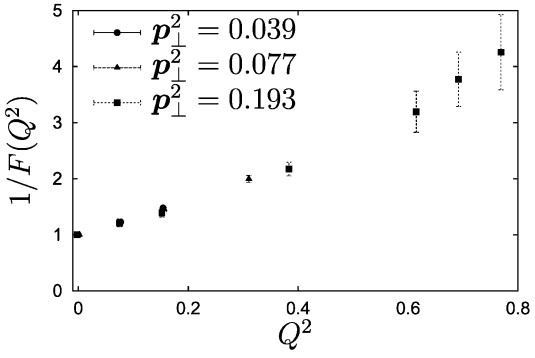

(a) $m_\pi = 0.511$

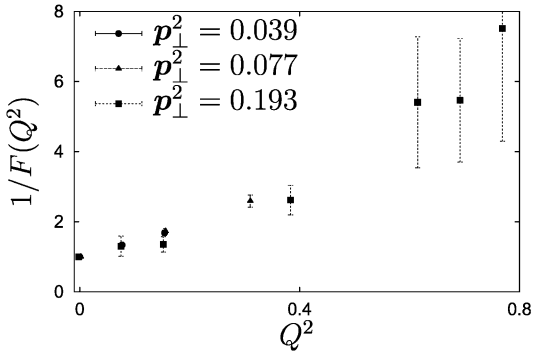

(b) $m_\pi = 0.283$

Fig. 3. The inverse of the vertex function F as a function of Q^2

line, but with larger error bars as well. When comparing data from the different transverse momenta sets, we see that the higher $\mathbf{p}_\perp^2$ values have larger error bars and for the lighter mass are more scattered around a straight line.

Figure 4 shows all our results, appropriately averaged over the different $\mathbf{p}_\perp^2$ values, together with the monopole fits. For the lightest pion mass, the fluctuations for the higher $\mathbf{p}_\perp^2$ values were too strong to allow for a reliable extraction of the vertex function at large Q^2 values. As expected, $F(Q^2)$ drops off more rapidly as the pion mass decreases. The fits deviate more strongly from the data at higher Q^2 for the lighter pions. As shown in Table 1b, the extracted parameter m_V agrees quite well with the corresponding fit parameter extracted at $T = 0$. Both lie close to the free ρ mass obtained from lattice QCD in [18]. This agreement with m_ρ gets better as the pion mass decreases towards the physical value. Our fit at $T = 0.93\,T_\mathrm{c}$ thus in general supports the simple VMD picture for the low Q^2 data also at a temperature just below T_c. A more detailed look at the function F is taken in Fig. 5. The two different pion masses show how the difficulties to extract information about F increase as the pion mass decreases. However, within the error bars, both examples again show that there is no overall significant difference to the form factor $F(Q^2)$ we extracted at $T = 0$. This is in contrast to most theoretical expectations based on effective models. In terms of the mass parameter m_V of our monopole fit, our results therefore do not support a significant dropping of the vector meson mass as T increases to $0.93\,T_\mathrm{c}$, at least not for the state with the lowest screening mass we project out by our spatial correlators.

By identifying the vertex function $F(Q^2, m_{\mathrm{sc},T})$ at $T = 0.93\,T_\mathrm{c}$ with the form factor of a pion embedded in a heat bath, we can also translate our findings into statements about its spatial extension and mean square radius. Figure 6 shows $\langle r^2 \rangle$ as obtained from the slope of F at $Q^2 = 0$, using the VMD parameterization. Both the $T = 0$ and $T = 0.93\,T_\mathrm{c}$ data lead to the same picture. There is no significant difference between the value for $\langle r^2 \rangle$ and in the dependence on the pion mass for both temperatures. Using the VMD parametrization and extrapolating the 'ρ' mass

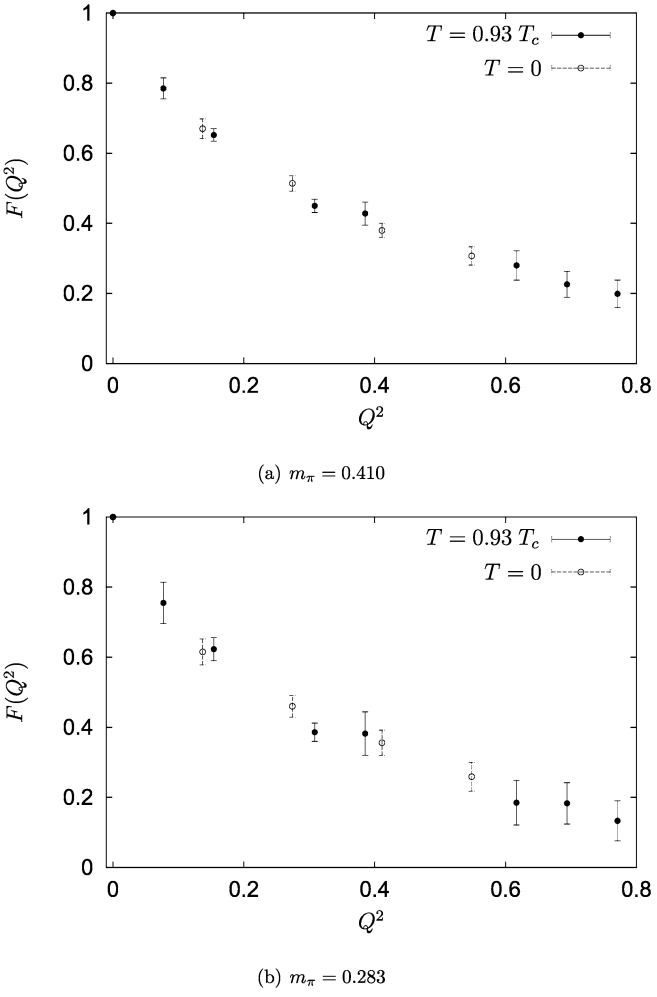

Fig. 5. The vertex function F compared with the form factor at $T = 0$

m_V, linearly in m_π^2, to the physical limit, we arrive at a value for $\langle r^2 \rangle$ that is about 15% below the experimental value for a free pion [25]. This small discrepancy could be due to the quenched approximation. However, Alexandrou et al. [26] have calculated density–density correlations in

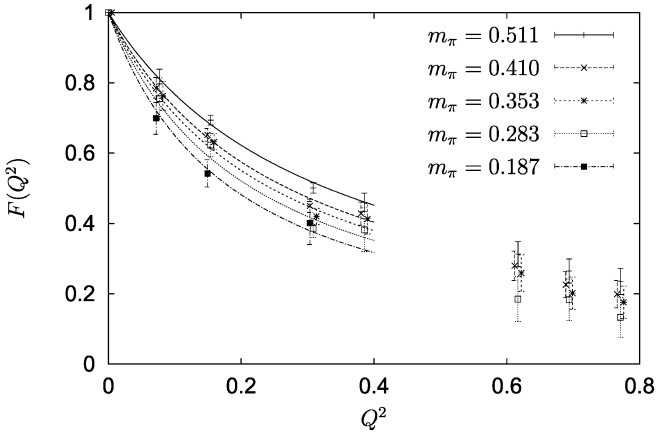

Fig. 4. The vertex function for different pion masses. *Curves*: fits to the VMD model

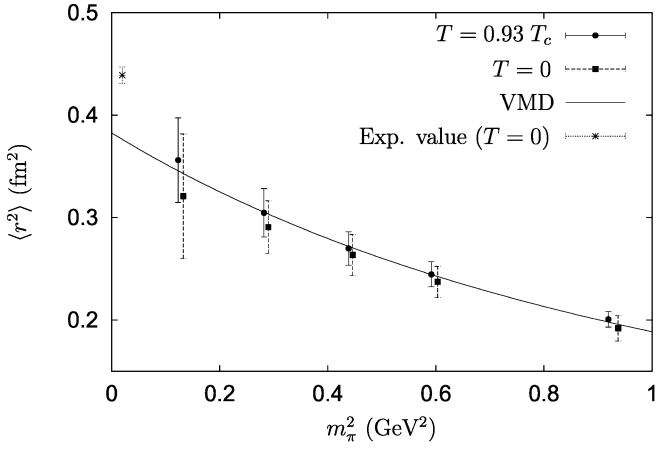

Fig. 6. The pion 'radius' at $0.93T_\mathrm{c}$ as a function of its mass

quenched as well as unquenched QCD at $T = 0$ and found only rather small effects for the pion. Recent unquenched calculations of the free pion form factor itself can be found in [27, 28].

6 Summary

In this paper, we have presented the first investigation of the electromagnetic vertex of a pion at finite temperature by means of numerical simulation. The temperature was chosen as $0.93\,T_c$, just below the critical temperature for the transition to the deconfined phase of QCD.

We considered two- and three-point functions for the pion for various transverse momenta. As the temporal extent of the lattice is limited by the inverse temperature we have calculated spatial correlators in the z-direction to study the dispersion relation and to extract the vertex functions of a pion embedded in a heat bath. For several quark masses we confirmed earlier findings that within errors the screening mass at $0.93\,T_c$ is the same as the free pion mass calculated on the lattice. Furthermore, except for the lightest pion and the largest momentum where errors are large, we could show that the dispersion relation for the lattice results was sufficiently well described by the continuum expression.

For the symmetrical kinematical conditions specifically chosen by us, the electromagnetic vertex of the pion can be described in terms of only a single vertex function $F(Q^2, m_{sc})$, which depends on the square of the photon four-momentum and the screening mass at the chosen temperature. For $T = 0$, this function is equal to the free pion form factor $F(Q^2)$. Within error bars, we found that for all quark masses and all Q^2 we considered, the vertex function agreed with the corresponding form factor at $T = 0$. Furthermore, we showed that at low Q^2 the vertex function for $T = 0.93\,T_c$ is well described by a monopole fit as suggested by a vector meson dominance model. The mass parameter m_V we extracted equals the fit parameter found earlier at $T = 0$ within errors. As the quark mass was decreased, this parameter was seen to approach the lattice value m_ρ for a ρ meson at $T = 0$. The simple vector meson dominance model thus remains a good description of the low Q^2 results also at a temperature close to T_c.

Our results on the pion vertex at low Q^2 can be translated into a mean square radius. Most effective models predict a pion radius which gradually increases with temperature. We do not find any significant change from the situation at $T = 0$. This may be due to the fact that, contrary to these models, our lattice results concern *screening* states. However, available lattice results have so far not shown appreciable differences between spatial and temporal pion two-point functions up to temperatures as high as investigated here and our findings based on the spatial three-point correlators may be more general.

To conclude, our results for the screening masses at $T = 0.93\,T_c$ confirm what earlier lattice studies of the pion had already shown. Our main new finding is that there is also no significant change in the vertex function F for screening states, a quantity that in contrast to the mass is directly sensitive to the internal structure of the pion. It will of course be interesting to continue these studies of the three-point functions to higher temperatures to see whether significant changes occur when T_c is crossed. Such studies are presently in progress [29].

References

1. H.J. Schulze, J. Phys. G **20**, 531 (1994)
2. C.A. Dominguez, M.S. Fetea, M. Loewe, Phys. Lett. B **387**, 151 (1996) [hep-ph/9608396]
3. C. Song, V. Koch, Phys. Rev. C **54**, 3218 (1996) [nucl-th/9608010]
4. A. Gomez Nicola, F.J. LLanes-Estrada, J.R. Pelaez, Phys. Lett. B **606**, 351 (2005) [hep-ph/0405273]
5. F. Karsch, E. Laermann, in: Quark gluon plasma III, ed. by R.C. Hwa et al. (2003), pp. 1–59 [hep-lat/0305025]
6. J. van der Heide, M. Lutterot, J.H. Koch, E. Laermann, Phys. Lett. B **566**, 131 (2003) [hep-lat/0303006]
7. J. van der Heide, J.H. Koch, E. Laermann, Phys. Rev. D **69**, 094 511 (2004) [hep-lat/0312023]
8. V. Koch, E.V. Shuryak, G.E. Brown, A.D. Jackson, Phys. Rev. D **46**, 3169 (1992) [hep-ph/9204236]
9. R.G. Edwards, U.M. Heller, T.R. Klassen, Nucl. Phys. B **517**, 377 (1998) [hep-lat/9711003]
10. B. Sheikholeslami, R. Wohlert, Nucl. Phys. B **259**, 572 (1985)
11. M. Lüscher, S. Sint, R. Sommer, P. Weisz, U. Wolff, Nucl. Phys. B **491**, 323 (1997) [hep-lat/9609035]
12. G. Martinelli, C.T. Sachrajda, A. Vladikas, Nucl. Phys. B **358**, 212 (1991)
13. M. Lüscher, S. Sint, R. Sommer, H. Wittig, Nucl. Phys. B **491**, 344 (1997) [hep-lat/9611015]
14. M. Guagnelli, R. Sommer, Nucl. Phys. Proc. Suppl. **63**, 886 (1998) [hep-lat/9709088]
15. L.H. Karsten, J. Smit, Nucl. Phys. B **183**, 103 (1981)
16. R. Gupta, D. Daniel, J. Grandy, Phys. Rev. D **48**, 3330 (1993) [hep-lat/9304009]
17. UKQCD, P. Lacock, A. McKerrell, C. Michael, I.M. Stopher, P.W. Stephenson, Phys. Rev. D **51**, 6403 (1995) [hep-lat/9412079]
18. M. Göckeler et al., Phys. Rev. D **57**, 5562 (1998) [hep-lat/9707021]
19. M.H. Quenouille, J. Roy. Stat. Soc. B **11**, 18 (1949)
20. J.W. Tukey, Ann. Math. Stat. **29**, 614 (1958)
21. E. Laermann, P. Schmidt, Eur. Phys. J. C **20**, 541 (2001) [hep-lat/0103037]
22. E. Laermann et al., Proceedings of SEWM04, 206
23. K. Barad, M. Ogilvie, C. Rebbi, Phys. Lett. B **143**, 222 (1984)
24. T. Bhattacharya, R. Gupta, W.-J. Lee, S.R. Sharpe, Phys. Rev. D **63**, 074 505 (2001) [hep-lat/0009038]
25. NA7, S.R. Amendolia et al., Nucl. Phys. B **277**, 168 (1986)
26. C. Alexandrou, P. de Forcrand, A. Tsapalis, Phys. Rev. D **66**, 094 503 (2002) [hep-lat/0206026]
27. D. Brommel et al., PoS **LAT2005**, 360 (2005) [hep-lat/0509133]
28. JLQCD, S. Hashimoto et al., PoS **LAT2005**, 336 (2005) [hep-lat/0510085]
29. J. van der Heide, J.H. Koch, E. Laermann, in preparation